Electric field compensation and sensing with a single ion in a planar trap

S. Narayanan,[1,2] N. Daniilidis,[1,2] S. A. Möller,[1,2,3] R. Clark,[2,4] F. Ziesel,[5] K. Singer,[5] F. Schmidt-Kaler,[5] and H. Häffner[1,3,a)]
[1]*Department of Physics, University of California, Berkeley, California 94720, USA*
[2]*Institut für Quantenoptik and Quanteninformation, Innsbruck, Austria*
[3]*Materials Sciences Division, Lawrence Berkeley National Laboratory, Berkeley, California 94720, USA*
[4]*Center for Ultracold Atoms, Massachusetts Institute of Technology, Cambridge, Massachusetts 02139, USA*
[5]*Institut für Physik, Universität Mainz, Mainz, Germany*

(Received 9 June 2011; accepted 1 November 11; published online 12 December 2011)

We use a single ion as a movable electric field sensor with accuracies on the order of a few V/m. For this, we compensate undesired static electric fields in a planar radio frequency trap and characterize the static field and its curvature over an extended region along the trap axis. We observe a strong buildup of stray charges around the loading region on the trap resulting in an electric field of up to 1.3 kV/m at the ion position. We also find that the profile of the stray field remains constant over a time span of a few months. © *2011 American Institute of Physics*. [doi:10.1063/1.3665647]

INTRODUCTION

Laser-cooled trapped ions offer a very high level of control, both of their motional and internal quantum states. At the same time, the large charge-to-mass ratio of ions makes their motion very sensitive to electric fields, both static and oscillatory. Thus, trapped ions recently emerged as a tool in small-force sensing.[1,2] More common applications of trapped ions are in quantum information science[3,4] and frequency metrology.[5,6] All of these applications can benefit from scalable ion-trap architectures based on microfabricated ion traps.

In particular, a promising route to achieve scalable quantum information processing uses complex electrode structures.[3,7] Considerable effort is made in developing microfabricated trap architectures on which all trap electrodes lie within one plane.[8–15] These so-called planar traps facilitate creation of complex electrode structures and are, in principle, scalable to large numbers of electrodes. Moreover, this approach makes use of mature microfabrication technologies and is ideally suited to approaches involving hybrid ion-trap or solid-state systems.[16,17]

Despite the advantages of planar trap architectures, a number of issues remain unsolved. To achieve reasonably large trap frequencies, planar traps require shorter ion-electrode distances than conventional three-dimensional traps.[8] This results in high motional heating rates for the ions[18–20] and causes charge buildup via stray light hitting the trap electrodes.[21] In addition, the proximity of the charges increases the effect of charge buildup as compared to macroscopic three-dimensional traps. Finally, planar traps do not shield stray electrostatic fields from the environment surrounding the trap as well as the three-dimensional trap geometries tend to do. Combined, these effects make the operation of planar traps much more sensitive to uncontrolled charging effects.

To harness the full advantages of segmented ion traps, ion-string splitting and ion shuttling operations are required.[4,22] For the reliable performance of these operations, control of the electrostatic environment over the full trapping region is necessary. Typically, one employs numerical electrostatic solvers to determine the potential experienced by the ions and generates electrode voltage sequences that will perform the desired ion shuttling.[23,24] Stray electrostatic fields, however, displace the ions from the radio frequency (RF)-null of the trap and thus introduce so-called micromotion,[25] sometimes to the point where trapping is no longer feasible. Thus, precise characterization and compensation of stray electric fields in the trapping region is required.

Conventional methods to sense and compensate the electric stray fields cannot easily be extended to planar traps because typically the stray fields are quantified via the Doppler shift induced by the micromotion. It is undesirable to scatter UV light from the trap electrodes, and thus for planar traps, the detection laser typically does not have a sizable projection on the motion perpendicular to the plane of the trap. We address these issues by applying a new method to compensate for stray fields well suited for planar trap geometries.[26,27]

Based on the voltages required to compensate the stray fields, we realize a single-ion electric field sensor characterizing the electric stray fields along the trap axis. We extract the curvature of the stray electric field from the difference in the measured and estimated secular frequencies, and we find that it is consistent with the measured position variation of the stray electric field. We observe a strong buildup of stray charges around the loading region on the trap. We also find that the profile of the stray field remains constant over a time span of a few months. The strength of the electric stray field and its position on the trap is correlated with the high heating rates observed close to the loading region.[20]

EXPERIMENTAL SETUP

We use a planar trap with gold electrodes deposited on a sapphire substrate to trap single $^{40}Ca^{+}$ ions at a height of 240 μm above the trap plane, see Fig. 1. Ions are created via

a)Electronic mail: hhaeffner@berkeley.edu.

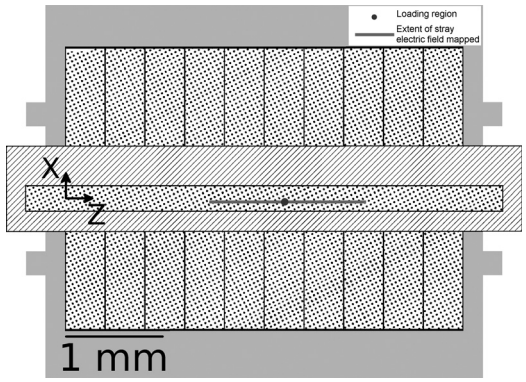

FIG. 1. Schematic of the trap used for the measurements.[20] The DC electrodes are shown as dotted region, the RF electrodes as diagonal lines, and the ground plane in gray. Details of the bonding pads to the dc electrodes are not shown for simplicity. The axes indicate the origin of the coordinate system. The line along the z axis on the central dc electrode indicates the range of axial positions in which the stray electric fields shown in Fig. 3 were measured. The circular mark on this line indicates the location used as a loading region, around which the highest increase in stray electric fields was observed.

two-step photoionization from a neutral calcium beam using 250 mW/cm^2 of laser light at 422 nm and 750 mW/cm^2 of laser light at 375 nm. Both the laser beams are focused to a waist size of 50 μm. Great care has been taken to minimize exposure of the trap surface to the neutral calcium beam.[20]

The RF electrode is driven at a frequency $\Omega/2\pi \approx 15$ MHz, amplified to 100mW and stepped up via a helical resonator in a quarter wave configuration to a voltage of approximately 100 V amplitude. A 2:1 asymmetry in the width of the RF electrode results in a tilt of the radio frequency quadrupole by approximately 16° in the xy plane. The dc electrodes are used to move the ion along the axial direction and to compensate the stray fields. The dc voltages used for trapping and compensation are between −10 V and 15 V. Typical secular frequencies in this work were $(f_{x'}, f_{y'}, f_z) \approx (1.2, 1.4, 0.4)$ MHz where the primes refer to the main trap axes, which are tilted with respect to the plane of the trap.

For Doppler cooling and detecting the ions, we use a diode laser at 794 nm, which is frequency doubled using a ring cavity to produce a wavelength of 397 nm. A second diode laser at 866 nm is used as a repump. Both lasers are frequency locked to cavities using the Pound-Drever-Hall method, and their frequencies can be varied by changing the cavity lengths with piezoelectric elements. The intensity of the detection laser at 397 nm is adjusted to about 40 mW/cm^2, and the intensity of the repump laser at 866 nm is adjusted to approximately 120 mW/cm^2. The Doppler cooling and repump lasers are overlapped and sent to the trap using a photonic crystal fiber. The laser beam is aligned almost parallel to the surface of the trap and forms an angle of approximately 45° with the x and z axes. Ion fluorescence is collected perpendicular to the trap plane using a lens system of NA = 0.29 and split between a PMT and CCD camera on a 90:10 beam splitter.

MINIMIZING MICROMOTION

In an ideal Paul trap, the ion is confined to a position at which the electric field caused by the oscillating drive voltage on the RF electrodes, is zero. Stray dc electric fields, however, push the ion off the RF node and the ion undergoes so-called micromotion driven by the oscillating RF field.[25] This motion causes broadening of the electronic transitions of the ion and, among other things, leads to a higher temperature limit for Doppler cooling.[3] In addition, micromotion can lead to the heating of trapped ions because of the noise present at the secular sidebands of the micromotion drive.[22,28] To position the ion on the RF node, the dc potential is carefully adjusted to minimize micromotion. Crucial to all minimization schemes is the efficient detection of micromotion in all three spatial directions.

Different techniques exist for fine-tuning the compensation of micromotion. The photon correlation method[14,25] relies on correlating the ion fluorescence to the phase of the RF field. In the resolved sideband method,[24,25] the sidebands of a narrow atomic transition are compared with the carrier transition to estimate the modulation index. Both methods are widely used to suppress micromotion in 3D traps. However, neither method can be easily extended to surface Paul traps because they directly use the Doppler shift induced by the ion motion. In the case of surface traps, the geometry typically limits the laser alignment to be in the plane parallel to the trap surface, resulting in no Doppler shift associated with the oscillations perpendicular to the trap surface unless one directs laser light onto the trap electrodes. However, it has been documented that UV light hitting the trap surface can lead to dramatic charge buildup even to the point where the trap becomes inoperable for days.[21] To circumvent this obstacle, the infrared repump light in $^{40}Ca^+$ has been used to detect the Doppler shift perpendicular to the trapping plane for micromotion compensation.[14] However, many ion species such as Mg^+, Al^+, Hg^+, Cd^+, and Be^+ do not have such transitions in the infrared, and other methods need to be employed.

Here we compensate the micromotion perpendicular to the trap plane with the following method. When the ion is displaced from the RF node, any voltage applied on the RF electrode creates an electric field at the ion position. If this voltage contains a frequency component that is in resonance with one of the ion secular frequencies, the ion can get excited in the direction of the secular mode provided that the driving field from the RF electrodes has some projection.[22] Experimentally, we find that large oscillation amplitudes of each of the three secular motions can be detected as a drop in ion fluorescence. The dynamics of ion fluorescence in the presence of the cooling laser and a resonant excitation are complex and go beyond the scope of this study.[29] Minimizing micromotion is achieved by shifting the ion position via dc potentials until the ion is in the RF minimum and cannot be excited by driving the RF electrode at any of the secular frequencies. This method is also being used by the NIST[26] and Osaska[27] ion trap groups.

Implementation

To implement this method, we first position the ion within 1 μm along the x direction from the RF null using the CCD camera and varying the RF amplitude. Further compensation in the x direction is achieved by reducing the

linewidth of the $S_{1/2}$-$P_{1/2}$ transition. For this, the detection laser intensity is adjusted close to saturation and red-detuned from the transition so that the fluorescence drops to half that of the value at the resonance. Then compensation voltages are adjusted to minimize the fluorescence. In our setup, both methods can only detect micromotion along the x direction, i.e., the direction that is parallel to the trap surface. For a very coarse compensation along the y direction (perpendicular to the trap surface), we keep the frequency of 397 nm and 866 nm laser on resonance and maximize the ion fluorescence by adjusting the compensation voltages.

Once a coarse compensation is achieved using the above method, we proceed with the method as outlined in the beginning of this section. Instead of exciting the secular frequency ω_i directly, we excite at a frequency $\Omega + \omega_i$.[22,28] To achieve this, the excitation signal from a function generator is mixed with the trap drive Ω before it is amplified and stepped up with a helical resonator, and scanned around $\Omega + \omega_i$. When the frequency of the excitation becomes resonant with $\Omega + \omega_i$, the ion heats up resulting in a decrease in fluorescence (see Fig. 2(a)).[22,27] A crucial requirement is that the step-up circuit that produces the high-voltage trap drive has a large enough bandwidth. The bandwidth of the helical resonator in our experiment is 270 kHz, and allows compensation with excitation frequencies up to an order of $\Omega \pm 2\pi \times 2$ MHz. The frequency of the Doppler cooling laser was chosen to be close to the $S_{1/2}-P_{1/2}$ transition to maximize sensitivity of the ion fluorescence to the ion kinetic energy. For the data presented in this paper, it was detuned about 3 MHz below the resonance, as compared to 20 MHz, which is roughly the natural linewidth of $^{40}Ca^{+}$.

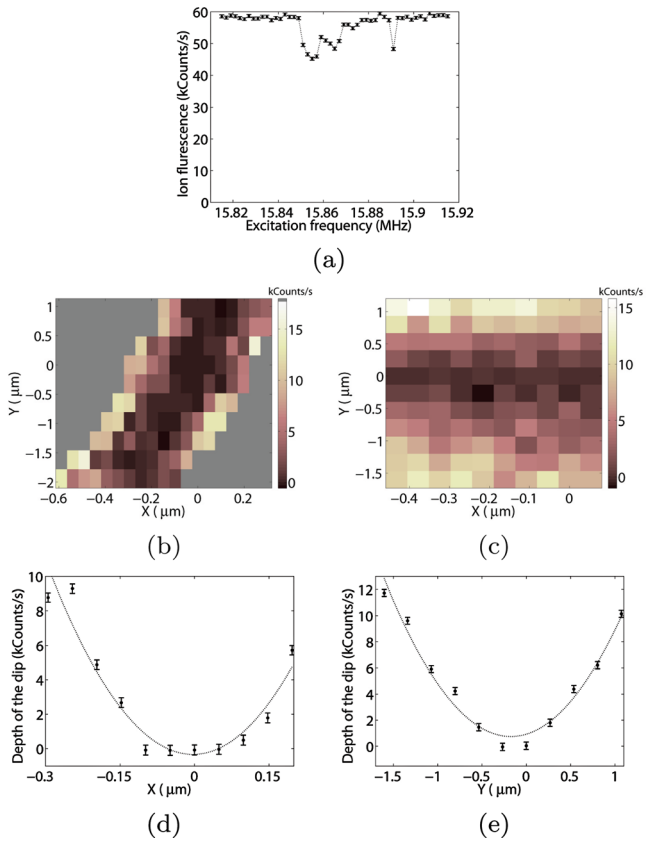

FIG. 2. (Color online) Micromotion compensation measurements. (a) Drop in ion fluorescence when the frequency of the additional excitation is equal to one of the secular frequencies of the ion. The dotted line is not a fit and is added as a guide for the eye. The dip value is estimated by averaging three values of ion fluorescence close to the excitation frequency. (b) and (c) Change in the dip depth for the excitation frequency $\Omega + \omega_x$ and $\Omega + \omega_y$, as a function of the ion position. (d) and (e) A cross section of (b) and (c), respectively, fitted with a parabola. Gray area in (b) is region without data because the excitation might drive the ion out of the trap. The darker the color the less excitation, i.e., less dip-depth was observed.

For compensation of micromotion in the x direction, the excitation signal is scanned repeatedly around $\Omega + \omega_x$ while adjusting the voltages on the dc electrodes such that between successive scans, the static electric field minimum moves predominantly in the x direction. The compensated position is reached when resonance of the excitation does not result in a decrease of fluorescence. The same process is repeated for compensation in the y direction. Results are shown in Fig. 2.

Figures 2(b) and 2(c) show the change in the dip depth when the excitation frequency is $\Omega + \omega_x$ and $\Omega + \omega_y$, respectively, as a function of ion position along the x and the y direction. The gray area in Fig. 2(b) is the region where no data is acquired because the excitation would drive the ion out of the trap. Figures 2(d) and 2(e) show cross sections of the 2D plots along the equilibrium positions of the ion when the DC saddle point moves along the x and y directions, respectively. The energy gain rate of the ion Γ is expected to be $\Gamma \sim E^2$, where E is the strength of the exciting electric field. We find that the data can be well fitted with a parabola, suggesting that for our experiments the dip depth is linear in the ion energy, whereas the electric field E can be described well as a quadrupolar field.

The accuracy of our measurements is estimated by calibrating the ion displacement as a function of change in the dc voltages using the CCD camera in the x direction and the detection laser in the y direction. These values were verified by modeling the displacement of the dc minimum with variation of the compensation voltages. By translating the applied voltage into actual displacement, we determine an accuracy of about 50 nm in the x direction and 300 nm in y direction in positioning the ion at the RF minimum. This corresponds to excess micromotion amplitudes of 6 nm and 40 nm in these respective directions. The accuracies could be further improved by increasing the excitation voltage and decreasing the frequency detuning of the detection laser from resonance.

One concern with this method is that in practical situations, the dc electrodes pickup RF voltage, the phase of which might be shifted, or which might depend on the RF excitation frequency. The reason for this is that the dc electrodes may capacitively couple to the RF electrode, with a frequency-dependent coupling determined by the filtering circuits connected to the dc electrodes. In our setup, we estimate the RF pickup of the excitation at $\Omega + \omega_i$ on the dc electrodes to differ by less than 20 μV from the pickup at Ω, which would shift the RF-null by about 15 pm, and thus not limit the accuracy.

ELECTRIC FIELD SENSING

It is instructive to extract the size and direction of the stray fields from the compensation voltages in various trapping

positions. We derive the stray field from the applied compensation voltages via an accurate electrostatic model of the trapping fields. Thus, determining the stray fields over an extended region yields important information for shuttling experiments or investigating the mechanism for charge buildup.

We model the trap potentials using the boundary element method solver CPO.[30] Because the radial trap axes are tilted, we determine the radial secular frequencies from a two-dimensional polynomial fit in the xy-plane. The agreement between experiment and simulation is better than 4%, corresponding to a disagreement of less than 20 kHz for axial secular frequency of 500 kHz, and 30 kHz for radial frequencies of between 1 and 2 MHz. We attribute the disagreement to details of the trap electrode geometry that were not included in the electrostatic simulation, as well as to the unknown curvature of the electrostatic stray fields. Only the spatially inhomogeneous part of the stray field will contribute to the discrepancy between simulation and experiment, because the electrostatic stray fields are compensated and included in the simulations, as we now describe.

The essential part of the stray field determination is to perform micromotion compensation as described above. After the compensation parameters have been determined, we measure the ion position along the z direction using the CCD imaging system. The values of the dc voltages at the compensated configuration and the ion position are then input to a minimization algorithm. The algorithm finds the stray field that results in the observed compensation parameters and position. The results are shown in Fig. 3.

The accuracy of our measurement scheme is limited by an estimated uncertainty of ± 2.5 μm in measuring the absolute ion position along the trap axis. This position uncertainty arises from the imprecision of the alignment of the microscope objective used for imaging with respect to the trap plane and from the size of trap features used to determine the position along the trap axis. This results in a systematic error of the electric field curves, mainly an offset of the entire curve. We find typical inaccuracies of $(\delta E_x, \delta E_y, \delta E_z) = \pm(5.5, 3, 15)$ V/m. The precision in determining the electric field at each ion position is on the order of a few V/m, and is limited by the precision to which the compensation parameters and relative ion position are determined. The errors from imperfect compensation lead to stray field imprecisions of ± 0.4 V/m in the horizontal direction and ± 2.5 V/m in the vertical direction, where we assume that the precision is limited by the ion displacement steps in Fig. 2.

The accuracy in determining the axial ion position at any given setting with respect to its positions in neighboring settings is limited by aberrations in the imaging optics and is estimated to be $\pm 0.1 \mu$m. This limitation leads to an imprecision of $\pm(2, 4, 0.5)$ V/m in the electric fields. The above limitations of the measurement leads to a total error of $\pm(7, 10, 16)$ V/m; however, the limitations are of a technical nature and can be further improved.

We performed this type of analysis over an extensive part of the trap. Measurements were performed during several months. The results obtained in the first weeks of trap installation in vacuum and trap operation were significantly different than those obtained later on. Initially, the magnitude of the stray electric fields in the radial directions varied on a day-to-day basis with a mean of 47 V/m and a standard deviation of 52 V/m. Measurements during that time were carried out only for one isolated axial ion position at 2240 μm. After two months of trap operation, there was an abrupt change in stray electric fields to considerably higher values. This change coincided with a pressure increase in the chamber to approximately 10^{-7} mbar because of a temporary ion pump failure. Subsequently, the stray field was mapped along the trap axis over a length of approximately 2 mm. The results are shown in Fig. 3. We measured stray fields as large as 1300 V/m. The curvature of the stray electric field is determined by comparing the measured secular frequencies with the estimated secular frequencies from the electrostatic solver. This curvature is found to be consistent with the derivative of the stray electric field. The results are plotted in Fig. 4.

Intuitively, it is conceivable that two localized charge sources located near the z axis are responsible for the observed electric field pattern. However, such inverse problems cannot be solved without further assumptions about the

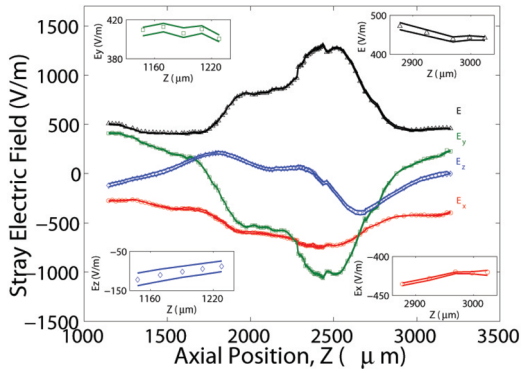

FIG. 3. (Color online) Stray electrostatic field along the trap axis. The three components E_x (○), E_y (□), E_z (◇), and the total electric field $E(\Delta)$ are shown. The solid curves on the two sides of each curve correspond to the possible systematic offset arising from the uncertainty in the absolute axial position, as described in the text. Insets are added to make the error in each of the stray electric field components visible.

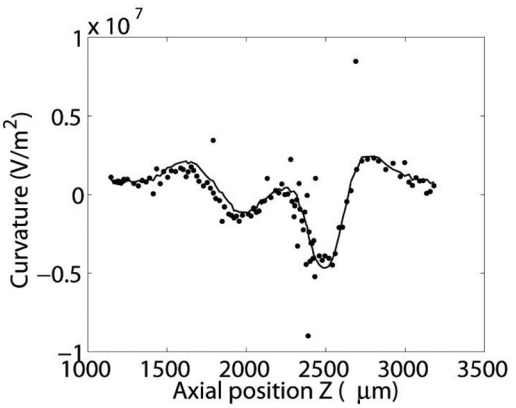

FIG. 4. The curvature of the stray electric field along the axis of the trap. The solid line is the estimated curvature using the change in the stray field and the dots (•) represent the curvature of the stray field as determined from the difference between measured and estimated secular frequencies.

charge distribution.[31,32] Attempts to reconstruct mathematically the charge distribution are in progress and will be reported elsewhere.

The position of the strongest electric field close to the most frequently used trapping positions suggests that electron and ion bombardment of the electrodes during the loading procedure or exposure to laser light caused the long-term charging. Finally, the high stray fields also appear to be spatially and temporally correlated with the observed high heating rate.[20]

Our measurement scheme allows us to monitor charging of the trap during operation. We found that the stray fields after the abrupt change in trap behavior are semi-permanent, showing a slow temporal drift on the order of tens of V/m per week. The most striking occurrence of this slow drift is the slight discontinuity in the data of Fig. 3 around an axial position of 2450 μm. This drift by 70 V/m, corresponding to a fractional change in the stray field by $\approx$6%, occurred over a period of nine days. Besides the slow drift of the stray field, short-term charging is observed in the course of a day. This is typically on the order of 100 V/m. When the laser light is turned off, discharging occurs over the course of several hours.

SUMMARY AND CONCLUSIONS

In this article, we demonstrate a simple, yet efficient method of measuring stray electric fields in planar ion traps. This method permits us to sense electric fields over an extended region, thus providing insight into the undesired charging of ion traps. This ability to characterize electric fields in the trapping region will be a valuable tool for evaluating planar ion traps, for developing ion loading approaches that minimize stray charging, and for compensating stray fields. We expect that this technique will be useful not only for scalable quantum information processing, but also for precision frequency metrology applications of trapped ions.

ACKNOWLEDGMENTS

The experiments are supported by the Austrian Ministry of Sciences with a START grant and by the Director, Office of Science, Office of Basic Energy Sciences, Materials Sciences and Engineering Division, of the U.S. Department of Energy under Contract no. DE-AC02-05CH11231. N. Daniilidis was supported by the European Union with a Marie Curie fellowship. F. Schmidt-Kaler acknowledges support from the German-Israel foundation and the EU network AQUTE.

[1]R. Maiwald, D. Leibfried, J. Britton, J. C. Bergquist, G. Leuchs, and D. J. Wineland, Nat. Phys. **5**(8), 551 (2009).
[2]M. J. Biercuk, H. Uys, J. W. Britton, A. P. VanDevender, and J. J. Bollinger, Nat. Nanotechnol. **5**(9), 646 (2010).
[3]D. J. Wineland, C. Monroe, W. M. Itano, D. Leibfried, B. E. King, and D. M. Meekhof, J. Res. Natl. Inst. Stand. Technol. **103**, 259 (1998).
[4]J. P. Home, D. Hanneke, J. D. Jost, J. M. Amini, D. Leibfried, and D. J. Wineland, Science **325**, 1227 (2009).
[5]P. O. Schmidt, T. Rosenband, C. Langer, W. M. Itano, J. C. Bergquist, and D. J. Wineland, Science, **309**(5735), 749 (2005).
[6]T. Rosenband, D. B. Hume, P. O. Schmidt, C. W. Chou, A. Brusch, L. Lorini, W. H. Oskay, R. E. Drullinger, T. M. Fortier, J. E. Stalnaker, S. A. Diddams, W. C. Swann, N. R. Newbury, W. M. Itano, D. J. Wineland, and J. C. Bergquist, Science **319**(5871), 1808 (2008).
[7]D. Kielpinski, C. Monroe, and D. J. Wineland, Nature **417**(6890), 709 (2002).
[8]J. Chiaverini, R. B. Blakestad, J. Britton, J. D. Jost, C. Langer, D. Leibfried, R. Ozeri, and D. J. Wineland, Quantum Inf. Comput. **5**, 419 (2005).
[9]S. Seidelin, J. Chiaverini, R. Reichle, J. J. Bollinger, D. Leibfried, J. Britton, J. H. Wesenberg, R. B. Blakestad, R. J. Epstein, D. B. Hume, W. M. Itano, J. D. Jost, C. Langer, R. Ozeri, N. Shiga, and D. J. Wineland, Phys. Rev. Lett. **96**, 253003 (2006).
[10]J. Britton, D. Leibfried, J. Beall, R. B. Blakestad, J. J. Bollinger, J. Chiaverini, R. J. Epstein, J. D. Jost, D. Kielpinski, C. Langer, R. Ozeri, R. Reichle, S. Seidelin, N. Shiga, J. H. Wesenberg, and D. J. Wineland, e-print arXiv:quant-ph/0605170 (2006).
[11]C. E. Pearson, D. R. Leibrandt, W. S. Bakr, W. J. Mallard, K. R. Brown, and I. L. Chuang, Phys. Rev. A **73**, 32307 (2006).
[12]J. Labaziewicz, Y. Ge, P. Antohi, D. Leibrandt, K. R. Brown, and I. L. Chuang, Phys. Rev. Lett. **100**, 13001 (2008).
[13]D. R. Leibrandt, J. Labaziewicz, R. J. Clark, I. L. Chuang, R. Epstein, C. Ospelkaus, J. Wesenberg, J. Bollinger, D. Leibfried, D. Wineland, D. Stick, J. Sterk, C. Monroe, C.-S. Pai, Y. Low, R. Frahm, and R. E. Slusher, Quantum Inf. Comput. **9**(11), 0901 (2009).
[14]D. T. C. Allcock, J. A. Sherman, D. N. Stacey, A. H. Burrell, M. J. Curtis, G. Imreh, N. M. Linke, D. J. Szwer, S. C. Webster, A. M. Steane, and D. M. Lucas, New J. Phys. **12**(5), 053026 (2010).
[15]J. M. Amini, H. Uys, J. H. Wesenberg, S. Seidelin, J. Britton, J. J. Bollinger, D. Leibfried, C. Ospelkaus, A. P. VanDevender, and D. J. Wineland, New J. Phys. **12**(3), 033031 (2010).
[16]L. Tian, P. Rabl, R. Blatt, and P. Zoller, Phys. Rev. Lett. **92**(24), 247902 (2004).
[17]N. Daniilidis, T. Lee, R. Clark, S. Narayanan, and H. Häffner, J. Phys. B **42**, 154012 (2009).
[18]Q. A. Turchette, Kielpinski, B. E. King, D. Leibfried, D. M. Meekhof, C. J. Myatt, M. A. Rowe, C. A. Sackett, C. S. Wood, W. M. Itano, C. Monroe, and D. J. Wineland, Phys. Rev. A **61**, 63418 (2000).
[19]L. Deslauriers, S. Olmschenk, D. Stick, W. K. Hensinger, J. Sterk, and C. Monroe, Phys. Rev. Lett. **97**(10), 103007 (2006).
[20]N. Daniilidis, S. Narayanan, S. Möller, R. Clark, T. Lee, P. Leek, A. Wallraff, St. Schulz, F. Schmidt-Kaler, and H. Häffner, New J. Phys. **13**, 013032 (2011).
[21]M. Harlander, M. Brownnutt, W. Hänsel, and R. Blatt, New J. Phys. **12**(9), 093035 (2010).
[22]R. B. Blakestad, C. Ospelkaus, A. P. VanDevender, J. M. Amini, J. Britton, D. Leibfried, and D. J. Wineland, Phys. Rev. Lett. **102**(15), 153002 (2009).
[23]S. Schulz, U. Poschinger, K. Singer, and F. Schmidt-Kaler, Fortschr. Phys. **54**, 648 (2006).
[24]F. Schmidt-Kaler, S. Schulz, U. Poschinger, and F. Ziesel, New J. Phys. **10**, 045007 (2008).
[25]D. J. Berkeland, J. D. Miller, J. C. Bergquist, W. M. Itano, and D. J. Wineland, J. Appl. Phys. **83**(10), 5025 (1998).
[26]T. Rosenband, Technical report, private communication (2009).
[27]Y. Ibaraki, U. Tanaka, S. Urabe, Appl Phys B **105**, 219 (2011).
[28]D. J. Wineland, C. Monroe, W. M. Itano, B. E. King, D. Leibfried, D. M. Meekhof, C. Myatt, and C. Wood, Fortschr. Phys. **46**(4-5), 363 (1998).
[29]N. Akerman, S. Kotler, Y. Glickman, Y. Dallal, A. Keselman, and R. Ozeri, Phys. Rev. A **82**(6), 3 (2010).
[30]See www.electronoptics.com for more information about CPO.
[31]B. Bosco and M. T. Sacchi, Ann. Phys. **12**, (1981).
[32]T. B. Smith, Inverse Probl. **1**(2), 173 (1985).